



Mesoporous geopolymer for improved adsorption and immobilization of copper ions

Zefeng Yu, Weifeng Song*, Peifei Ding

School of Environmental Science and Engineering, Guangdong University of Technology, Guangzhou 510006, China, emails: weifengsong@gdut.edu.cn (W. Song), 578514928@qq.com (Z. Yu), 653762306@qq.com (P. Ding)

Received 10 October 2019; Accepted 2 April 2020

ABSTRACT

In this study, a new type of geopolymer was prepared via hydrothermal method using metakaolin as raw material. The Cu(II) adsorption property of the obtained geopolymer composite was investigated. At a 4/6 Al/Si ratio, the geopolymer exhibited optimal adsorption performance. Microstructural and morphological changes were characterized via Fourier-transform infrared spectroscopy, scanning electron microscopy, and X-ray diffraction. The optimal adsorption capacity of the geopolymer was 97.58 mg/g. Adsorption kinetics and isotherms were in accordance with the pseudo-second-order and Freundlich isotherm models, respectively. The specific surface area of the geopolymer was 32.16 m²/g, whereas that of the raw material was 10.07 m²/g. The pore size of the obtained geopolymer composite decreased after five regeneration cycles. After specific adsorption experiments, the geopolymer was recovered via immobilization. The adsorption rate of the recycled geopolymer after five regeneration cycles was maintained above 95% with immobilization efficiency of 99%. This study provides valuable theoretical guidance for the adsorption of metals.

Keywords: Geopolymer; Adsorption; Immobilization; Copper ion; Mesoporous

1. Introduction

In the field of environmental science, the term metals mainly refer to metal elements in the environment that can be enriched in the process chain, which produces a modified final product. Conventional methods to treat metal-containing wastewater convert metal ions in solution to their solid-state, which can be relatively easily separated from the wastewater. Chemical precipitation and adsorption [1,2] are commonly used methods to perform this procedure. Various types of adsorption materials have been researched, particularly: natural clay [3], fly ash [4], and red mud [5]. Due to their high adsorption capacity, high specific surface area, an abundance of raw materials, and low cost, these materials are environmentally friendly and, therefore, widely used for the removal of metals [6].

Geopolymers, also known as soil polymers or inorganic polymers, belong to a type of aluminum silicate solid that was first proposed by Davidovits et al. [7]. The formation of the geopolymer structure requires the breakage of the Si–O and Al–O bonds in the raw material form of the precursor [8]. The obtained material is then dehydrated and condensed, thus forming a covalent bond structure with the O-connected silicon tetrahedron and aluminum tetrahedron. Due to their notable advantages such as good stability in aqueous solution, low-cost, and complete lack of secondary pollution, researchers have increasingly focused on the metal adsorption properties of geopolymers [9]. After the metal adsorption, the adsorbent can be recovered via leaching in acidic solution, thus being a regenerative geopolymer. However, the adsorption capacity of recovered

* Corresponding author.

geopolymers after several regeneration cycles strongly decreases, no longer meeting the requirements. In this context, the hydrothermal reaction is an emerging method for geopolymer regeneration, and it is a basic procedure during geopolymer synthesis. During the regeneration process, adsorbed metal ions are firmly immobilized and new adsorption sites are formed on the geopolymer surface. The regenerated geopolymer can be used for landfill, which is considered simple and feasible [10].

The present work studies the synthesis conditions and properties characteristics of a new type of geopolymer composite derived from metakaolin, NaAlO_2 , and Na_2SiO_3 as source materials. Sodium hydroxide (NaOH) was added as the activating agent during sample preparation. Cu(II) adsorption by the obtained geopolymer under different synthesis conditions was investigated. Furthermore, the kinetics of Cu(II) adsorption and feasibility of geopolymer regeneration were evaluated. A regeneration test was conducted to evaluate the renewability properties.

2. Materials and methods

2.1. Materials

The metakaolin used for this study was obtained via kaolinite dehydration at 900°C in a muffle furnace for 1 h, and its main chemical elements are listed in Table 1. Distilled water and analytical grade NaOH , Na_2SiO_3 , and NaAlO_2 were used for all experiments.

2.2. Sample preparation

The sample preparation process started by mixing NaAlO_2 and Na_2SiO_3 at a designed molar ratio (Al/Si), to which 4 g of metakaolin were added. This sample was then

mixed with a prepared alkaline solution at a pre-designed concentration and 0.1 solid/solution weight ratio, thus forming the geopolymer precursor. This precursor was then cast into a reactor, which was heated to a designated temperature in the muffle furnace to initiate the hydrothermal reaction. After the reaction, solid particles were filtered and washed with distilled water until neutralization.

To examine the influence of the geopolymer composition on its adsorption properties, several parameters were varied during the sample preparation. Excluding the always fixed solid-liquid ratio, four series of synthesis parameters were varied in this study: (1) the pre-designed molar ratio of Al/Si ; (2) the concentration of the alkaline solution, which ranged from 0.2 to 1.4 mol/L; (3) the activating temperature for the hydrothermal reaction, which ranged from 20°C to 180°C ; (4) the activating time of the hydrothermal reaction, which varied from 10 to 360 min. The details of various synthesis parameters are summarized in Table 2.

To analyze the adsorption efficiency of the prepared geopolymer, batch experiments were conducted. To explore the effects of contact time, 0.05 g of adsorbent was added to 50 mL of a 100 mg/L Cu(II) solution. The pH of the solution was controlled at 5.5, and the bottle was sealed. Finally, the mixture was placed in a gas bath shaker for different contact times (2.5–150 min) at 25°C and 150 rpm. Each series of experiments was performed in triplicate. After filtration, atomic absorption spectroscopy was used to analyze the filtrate and to measure the amount of metal extracted from the solution. To explore the effect of initial Cu(II) concentration in a solution, 0.05 g of adsorbent was added to 50 mL of different Cu(II) concentration (10–100 mg/L) solutions. The amount of metal ion adsorbed by the geopolymer was calculated using Eq. (1):

$$q_e = \frac{(C_0 - C_e)V}{m} \quad (1)$$

where C_0 is the initial concentration (mg/L) of the metal solution, C_e is the equilibrium adsorption concentration (mg/L), q_e is the equilibrium adsorption amount (mg/g), m is the adsorbent mass (mg), and V is the solution volume (mL).

2.3. Geopolymer characterization

The surface morphology of the geopolymer was observed via scanning electron microscopy (SEM; JEOL, JSM-5600LV, Japan). Functional groups were characterized via Fourier-transform infrared spectroscopy (FT-IR; Thermo Fisher, Nicolet 6700, USA). The elemental composition was analyzed

Table 1
Chemical composition of the studied metakaolin

Component	Content (wt.%)
SiO_2	49.03
Al_2O_3	45.48
TiO_2	0.67
Fe_2O_3	0.51
CaO	0.51
ZrO_2	0.10
Loss amount	3.70

Table 2
Synthesis parameters for sample preparation

Series set	Varied parameter	Fixed parameters
1	Molar ratio of Al/Si = 9:1, 8:2, 7:3, 6:4, 5:5, 4:6, 3:7, 2:8, and 1:9	4:6
2	Alkaline concentration = 0.2–1.4 mol/L	0.8 mol/L
3	Temperature = 20°C – 180°C	160°C
4	Curing time = 10–360 min	120 min

via X-ray fluorescence spectroscopy (Shimadzu, XRF-1800, Japan). The internal geopolymer structure was characterized via X-ray diffraction (XRD) using a Brook D8-XRD-7000 (Germany) advance X-ray powder diffractometer. Finally, the specific surface area and micropore structure were analyzed by an automatic surface and porosity analyzer (Micromeritics, ASAP2020, USA).

2.4. Regeneration tests

After the adsorption experiment, the specimens were filtered by a membrane and dried for 1 h at 65°C to produce geopolymer residues, which were collected and used as samples for the regeneration tests. To perform a regeneration cycle, the collected samples were first mixed with the activation solution (NaOH:Na₂SiO₃:NaAlO₂ = 6:6:4) at a designated mass ratio. Subsequently, the hydrothermal process was conducted in a muffle furnace under 160°C for 2 h to achieve geopolymer regeneration. The obtained residue was collected via membrane filtration, and it was washed several times with deionized water until a pH of 7 was obtained. When the neutralization was finished, the residue was used in adsorption experiments, following the procedure described in section 2.4. To ascertain the reusability of the geopolymer, five regeneration cycles were conducted under similar preparation methods.

The immobilization rate of Cu(II) can be calculated by Eqs. (2) and (3), and the immobilization efficiency (mg/g) by Eq. (4):

$$b = \frac{m_1 - m_2}{m_1} \times 100\% \quad (2)$$

$$m_2 = cV \quad (3)$$

$$G = \frac{m_1 - m_2}{m} \quad (4)$$

where m_1 (mg) is the mass of Cu(II) absorbed by the geopolymer, m_2 (mg) is the Cu(II) mass in the reclaimed liquid, c (mg/L) is the concentration of Cu(II) in the regenerated liquid, V (L) is the volume of the regenerated liquid, and m (g) is the quality of the recycled geopolymer.

3. Results and discussion

3.1. Effect of synthesis conditions on sorption behavior

The correlation between the Al/Si ratio and adsorption capacity is shown in Fig. 1a. The results show that the adsorption capacity was enhanced when the Al/Si ratio decreased from 9/1 to 4/6, at which the optimal result was obtained. The adsorption capacity was also enhanced with increased alkaline concentration and, according to Fig. 1b, the optimal concentration of the NaOH solution was 0.8 mol/L.

The variation curves of adsorption capacity and reaction temperature are shown in Fig. 2a. The adsorption capacity of the obtained geopolymer greatly improved when the activation temperature exceeded 100°C. The optimal Cu(II) adsorption capacity was 96.66 mg/g, achieved at 160°C. Geopolymers are typically formed at 100°C. Thus, they can be considered an energy-saving adsorbent. Furthermore, high-quality geopolymers can be obtained after activation using metakaolin or fly ash as raw material.

The correlation between geopolymer adsorption capacity and the activation time is shown in Fig. 2b. During the initial stage of the reaction, the adsorption rate did not reach 50 mg/g within 80 min. At that stage and in the presence of the activator, metakaolin was more likely to form a precursor. As the activation time reached 80–120 min, the geopolymer rapidly formed, resulting in a sharp increase in Cu(II) adsorption, which reached 96.66 mg/g. The activation process was completed within 120 min, and there was a slow improvement in the adsorption capacity with increasing reaction time.

3.2. FT-IR analysis

The FT-IR results for metakaolin and geopolymer are shown in Fig. 3. Compared to metakaolin, the geopolymer band shifted to a higher wavenumber, and the transmittance decreased [11].

The analysis of the FT-IR results indicates that the change of absorption peak appears within the 950 and 1,200 cm⁻¹ bands. The change from 950 to 1,200 cm⁻¹ can be ascribed to the change of asymmetric stretching vibration caused by the Si–O–Si skeleton. The 1,094 cm⁻¹ absorption peak of Si–O–Si noticeably changed. The absorption peak shifted to 1,166 and 1,102 cm⁻¹, while the intensity strongly

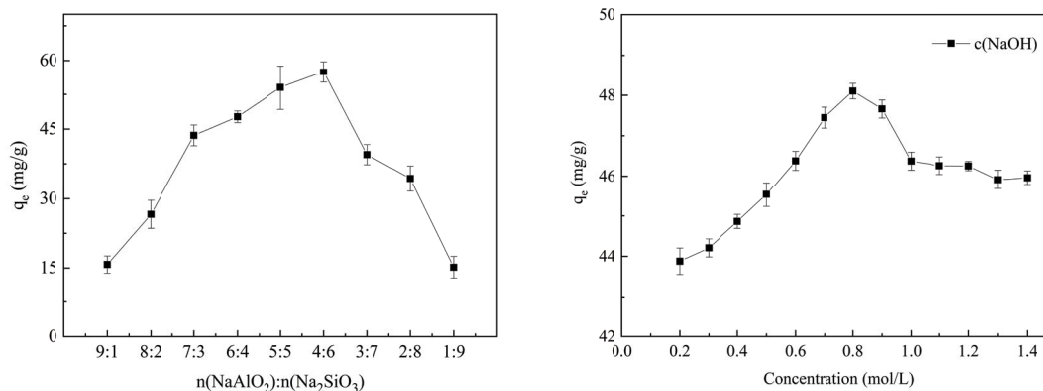


Fig. 1. Correlation between reaction conditions and adsorption capacity (a) Al/Si ratio and (b) NaOH concentration.

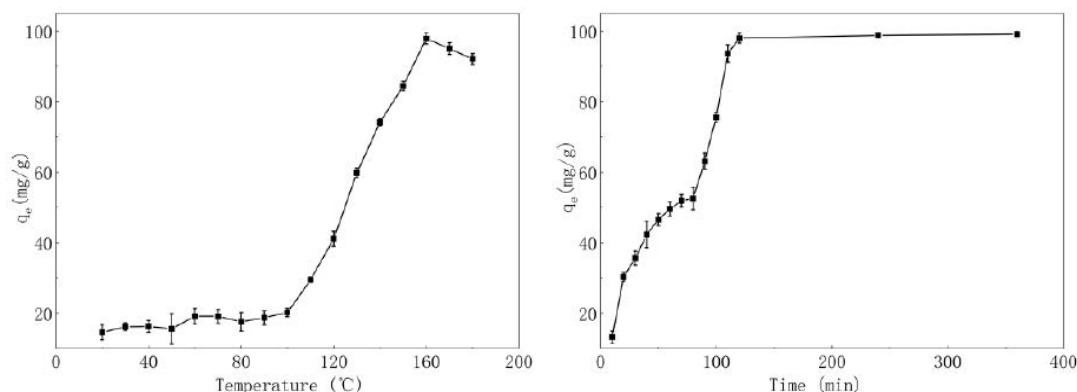


Fig. 2. Correlation between reaction conditions and adsorption capacity (a) temperature and (b) time.

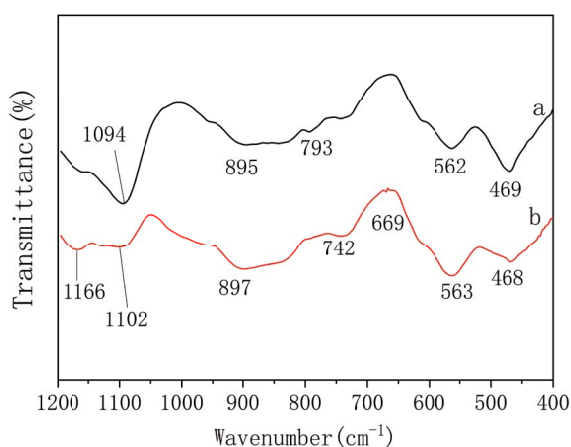


Fig. 3. FT-IR of (a) metakaolin and (b) geopolymer.

decreased, which indicates that the Si–O structure was reorganized due to the activating agent, and a new Si–O–Al structure was formed [12]. This formation occurred due to the dissolution of silicon and aluminum components, which formed an amorphous structure and replaced part of the Si by Al, thus forming the Si–O–Al structure [13]. The original absorption peak at 469 cm^{-1} shifted to 468 cm^{-1} due to the bending of Si–O and the structure of Al–O [14]. Therefore, the structure of the geopolymer was formed after the activation. In addition, Si–O antisymmetric stretching vibration was observed at 669 cm^{-1} .

3.3. SEM analysis

SEM images of the samples are shown in Fig. 4. The metakaolin surface is irregular and loose (Fig. 4a). After the hydrothermal reaction, the geopolymer was formed with many fine particles produced by the dissolution of metakaolin into microparticles due to the effect of the activating agent. On the metakaolin surface, aluminum and silicon tetrahedron exist in free form, where two tetrahedra share one oxygen atom [11]. Then, the first rapid polymerization of the Al–O–Si structure in oligomeric state occurred, followed by the formation of silicate on the surface of the slow coagulation process. The resulting structure of the

geopolymer is shown in Fig. 4b. Compared to metakaolin, the surface of the geopolymer was regular and compact.

3.4. XRD analysis

The XRD patterns of the metakaolin and geopolymer are shown in Fig. 5. The main crystal phases of metakaolin are mullite, sillimanite, iron cordierite, and calcium aluminate. After the hydrothermal reaction, the silicon and aluminum components in the raw materials formed a sodium aluminosilicate polymer (Na–PS) [15].

3.5. Pore size distribution

The pore size distribution is presented in Fig. 6. The majority of pore sizes remained below 2 nm. The largest pore size was 4.85 nm, and it accounted for the smallest proportion of distribution. Due to their small pore size, the adsorption resistance inside the pores was larger for metakaolin, which was not conducive to adsorption. In contrast, the pore size of the geopolymer was mostly around 15.98 nm. This larger pore size distribution indicates that the geopolymer possesses a higher surface area, which resulted in improved adsorption efficiency [16,17]. This result indicates that geopolymer is a mesoporous material.

3.6. Adsorption kinetics

To determine the optimal contact time between Cu(II) and the geopolymer, the Cu(II) adsorption capacities were measured as a function of contact time. First, 0.05 g of geopolymer was added to each flask containing 250 ml of Cu(II) solution at a concentration of 100 mg/L and a pH of 5.5. Then, the flasks were subject to constant shaking for 150 min. Fig. 7a shows that the amount of adsorbed Cu(II) increased with increasing contact time, and Cu(II) equilibrium was reached after 90 min. Therefore, 120 min was selected as the optimal contact time for all the following studies.

Pseudo-first- and pseudo-second-order kinetic models are commonly used to determine the factors that control adsorption rates and to observe the mechanism of metal adsorption onto geopolymers. Pseudo-second-order kinetics can be divided into three stages: (1) external liquid film adsorption, (2) surface adsorption, and (3) intraparticle

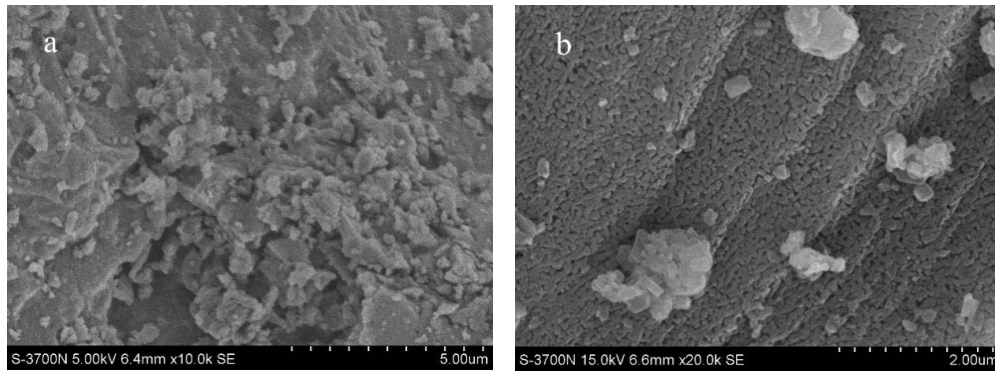


Fig. 4. SEM images of (a) metakaolin and (b) geopolymer.

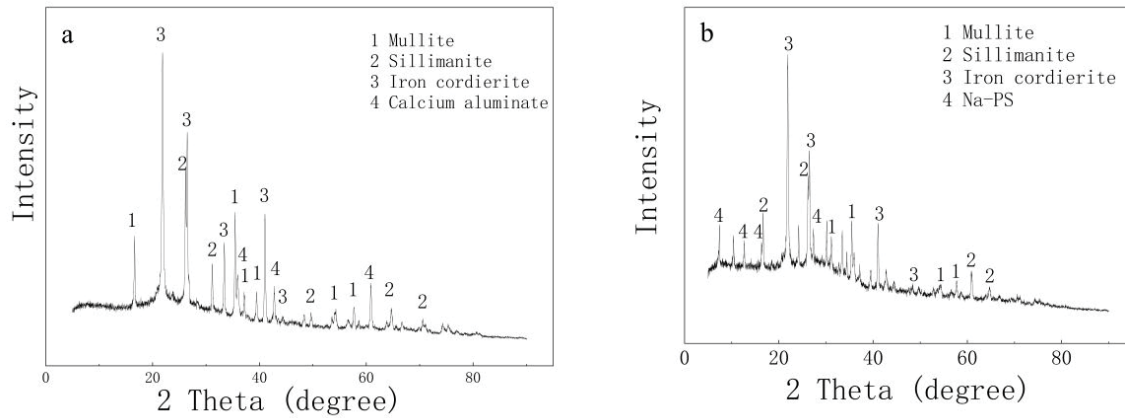


Fig. 5. XRD analyses of (a) metakaolin and (b) geopolymer.

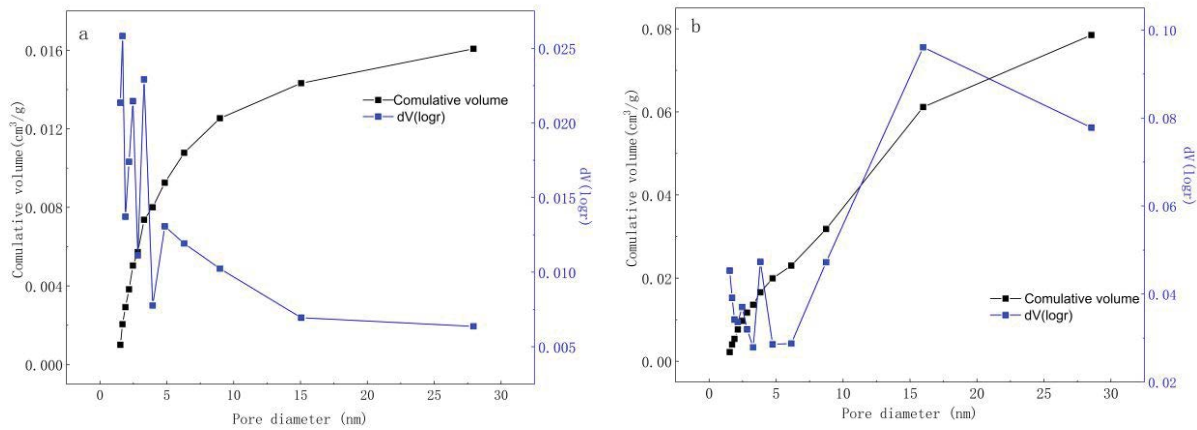


Fig. 6. The pore size distribution of (a) metakaolin and (b) geopolymer.

diffusion, which is commonly used to describe the adsorption of Cu(II) by the geopolymer. Pseudo-first-order kinetics as described by Lagergren is expressed in Eq. (5), and pseudo-second-order kinetics [18] in Eq. (6).

$$\log(q_e - q_t) = \log q_e - \frac{(k_1)t}{2.303} \tag{5}$$

$$\frac{t}{q_t} = \frac{1}{k_2 q_e^2} + \frac{t}{q_e} \tag{6}$$

where q_e (mg/g) and q_t (mg/g) represent the number of metal ions adsorbed on the geopolymer at equilibrium and at time t (min), respectively; and k_1 (min^{-1}) and k_2 [$\text{g}/(\text{mg min})$] are rate constants.

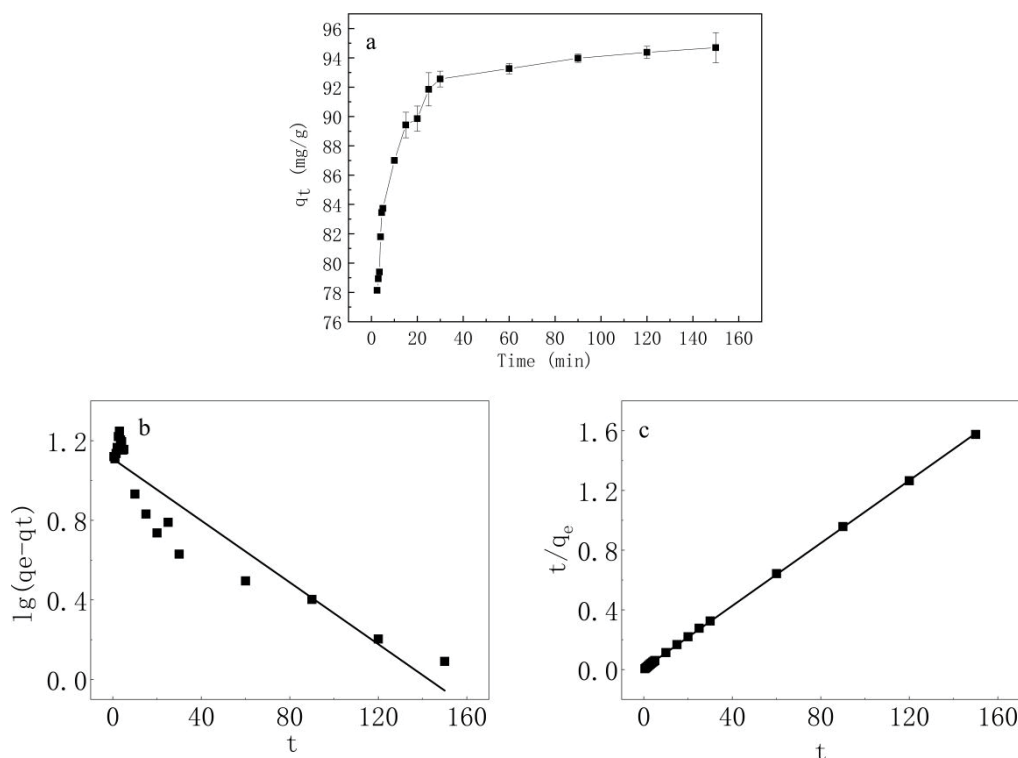


Fig. 7. (a) Adsorption kinetics of the geopolymer for Cu(II). Linear fitting of experimental data for (b) pseudo-first-order and (c) pseudo-second-order equations.

Linear fitting of the experimental data is shown in Figs. 7b and c, and the parameters calculated via Eqs. (5) and (6) are listed in Table 3. The theoretical q_e calculated from the pseudo-second-order model and the experimental q_e strongly overlapped. In addition, the determined coefficients (R^2) obtained from the pseudo-second-order kinetic model far exceeded those obtained from the pseudo-first-order model. Therefore, the experimental kinetic data agreed better with the pseudo-second-order kinetic model.

The Cu(II) adsorption capacity of different geopolymers and other types of adsorbents on the basis of previous articles are shown in Tables 4 and 5, respectively. Compared to other types of adsorbents, the geopolymer obtained in this study presented a large advantage, achieving a high adsorption capacity of 97.67 mg/g.

The Weber–Morris equation can be used to describe whether the mass transfer process occurred on the surface or internally [27]. As shown in Fig. 8, the plots fitting the results comprise four linear portions. Therefore, the adsorption of Cu(II) by the geopolymer comprised four stages,

according to the Weber–Morris model. The fitting results are summarized in Table 6. During the first 0.5 min, Cu(II) was rapidly adsorbed. However, the slope of the fitting curve at 0.5–3 min was negative, indicating that there was a release of Cu(II) at that time. The adsorption gradually saturated after 30 min. Except for the initial 0–0.5 min portion of the fitting curve, other intercepts did not cross the origin, indicating that a certain boundary layer thickness existed in the adsorption process.

3.7. Adsorption isotherms

At 120 min contact time and 5.5 pH, the initial concentration of the solutions containing Cu(II) were set to 10–100 mg/L. Fig. 9a shows that the initial concentration of Cu(II) ions was higher, and the equilibrium adsorption value was larger. These results might be attributed to the adsorption sites, which do not get saturated at low concentrations. With increasing metal concentration, the adsorption sites gradually become saturated. The maximum Cu(II) adsorption achieved by the geopolymer was 81.6 mg/g.

Table 3
Kinetic parameters for the adsorption of Cu(II) using geopolymers

$q_{e,exp}$ (mg/g)	Pseudo-first-order kinetics			Pseudo-second-order kinetics		
	q_e (mg/g)	k_1 (min ⁻¹)	R^2	q_e (mg/g)	k_2 (g/mg min)	R^2
97.67	65.64	0.0180	0.870	95.24	0.0156	0.999

Table 4
Cu(II) adsorption capacity of different geopolymers

Source of literature	Initial concentration of Cu(II) (mg/L)	Adsorption temperature (°C)	Adsorption capacity (mg/g)
Onutai et al. [19]	20	25	2.4
Andrejkovič et al. [20]	50	–	44.73
Singhal et al. [9]	–	–	40
Al-Harashsheh et al. [21]	160	25	57.9
This research	100	25	97.67

Table 5
Cu(II) adsorption capacity of different adsorbents

Adsorbents name	Maximum adsorption capacity (mg/g)	Source of literature
Poly(vinyl alcohol)/sodium alginate/KMnO ₄ modified biochar	87.07	Xiao et al. [22]
Sewage sludge-derived biochar	74.51	Tang et al. [23]
Modified chitosan gel incorporated with magnetic nanoparticle	90.99	Anush and Vishalakshi [24]
Superadsorbent hydrogel based on lignin and montmorillonite	74.88	Sun et al. [25]
Ligand based facial conjugate materials	174.76	Awual et al. [26]
Geopolymer	97.67	This research

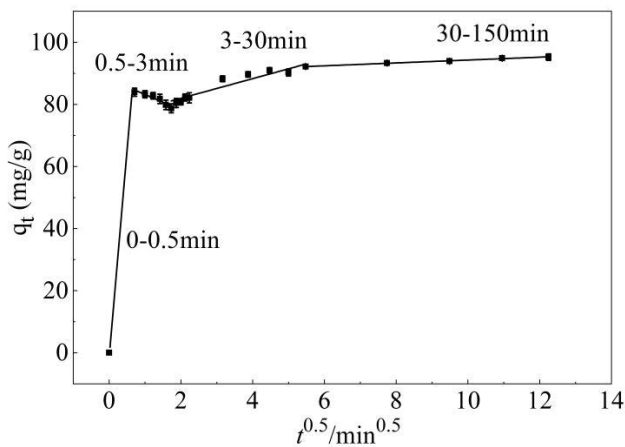


Fig. 8. Fitting of experimental data to the Weber–Morris equation.

To further investigate the geopolymer metal-adsorption behavior, additional experiments were performed at a constant temperature (25°C) and different concentrations of Cu(II). The expressions of the Langmuir Eq. (7) and Freundlich Eq. (8) models are given as:

$$\frac{C_e}{q_e} = \frac{1}{q_0 b} + \frac{C_e}{q_0} \quad (7)$$

$$\ln q_e = \ln K_f + \frac{1}{n} \ln C_e \quad (8)$$

Table 6
Fitting of experimental data on Cu(II) for different dynamic models

Simulation time period	Fitting model	Fitting equation	R ²
0.5–150 min	Lagergren	$y = -0.0078x + 1.109$	0.870
0.5–150 min	Ho	$y = 0.0105x + 0.00706$	0.999
0–0.5 min	Weber–Morris	$y = 117.76x$	1
0.5–3 min	Weber–Morris	$y = -4.996x + 88.18$	0.889
3–30 min	Weber–Morris	$y = 3.164 + 75.63$	0.899
30–150 min	Weber–Morris	$y = 0.4639x + 89.64$	0.973

where C_e is the equilibrium concentration of Cu(II) (mg/L), and q_e is the amount of adsorbed Cu(II) at equilibrium (mg/g). q_0 (mg/g) and b (L/mg) are both Langmuir constants that are associated with adsorption capacity and intensity, respectively. K_f and n are both Freundlich constants, which are related to adsorption capacity and intensity, respectively [28].

The linear fitting of two isotherm models is presented in Figs. 9b and c. The relevant isotherm parameters are summarized in Table 7. The obtained results indicate that the adsorption of Cu(II) on the geopolymer can be well described via the Freundlich model. According to the fitting results of the adsorption isotherm models, the Langmuir model is not adequate because the predicted adsorption capacity is significantly smaller than the actual adsorption capacity in the case of higher initial copper concentration (more than 70 mg/L). Compared to the Langmuir model, the Freundlich model achieves better correlation with the experimental data,

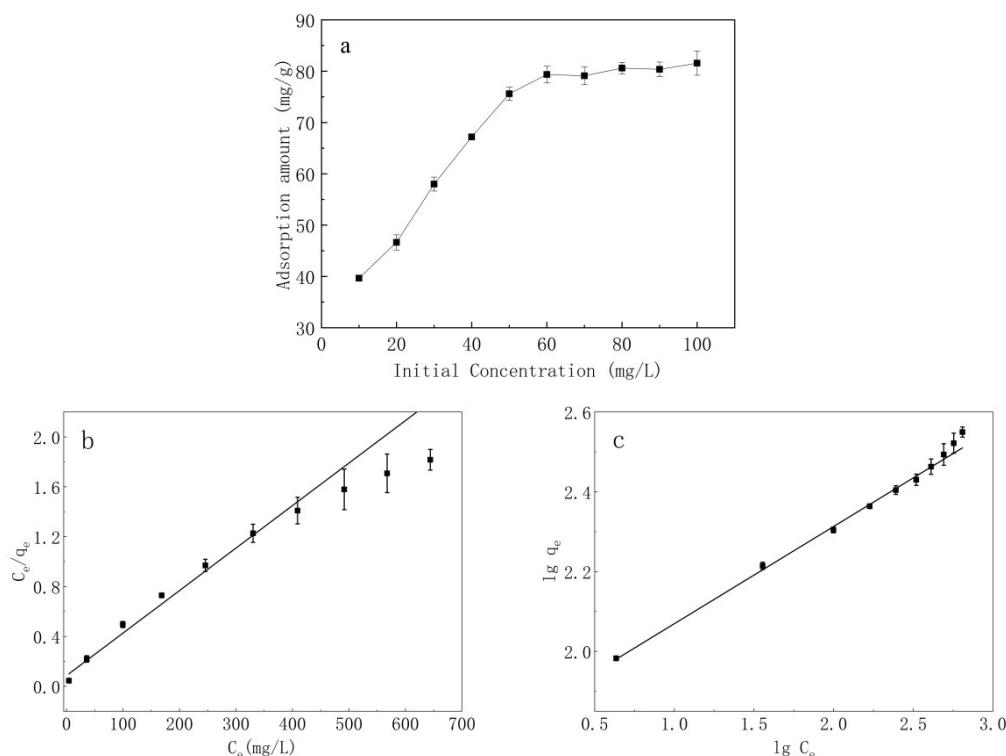


Fig. 9. (a) Experimental isotherms of the geopolymer towards Cu(II). (b) Langmuir and (c) Freundlich isotherms for the adsorption of Cu(II) onto the geopolymer.

Table 7
Parameters of Langmuir and Freundlich isotherms on Cu(II) adsorption

Langmuir			Freundlich		
q_0 (mg/g)	b	R^2	K_f (mg/g)	n	R^2
60.16	0.107	0.965	11.5	3.76	0.998

presenting an R^2 of 0.9959. From the fitting results, the value of n ranges between 1 and 10, indicating that the adsorption process can be well explained by the Freundlich isotherm [29]. Similar to the graphene-modified chitosan, the Cu(II) adsorption behavior of the obtained geopolymer is conformed to the multimolecular layer adsorption model [30].

3.8. Regeneration tests

3.8.1. Efficiency of regenerated geopolymer

Following the adsorption experiment, the reproducibility of the adsorbent was investigated based on the collected geopolymer. As the regeneration cycles were conducted, the adsorbed Cu(II) was immobilized in the newly emerged geopolymer under hydrothermal conditions. The adsorption curves of the regenerated composite are shown in Fig. 10. In contrast to general adsorbents [31], the geopolymer achieved good adsorption capacity towards Cu(II) after multiple regenerations. The Cu(II) removal efficiency and the immobilization of the regenerated geopolymer were

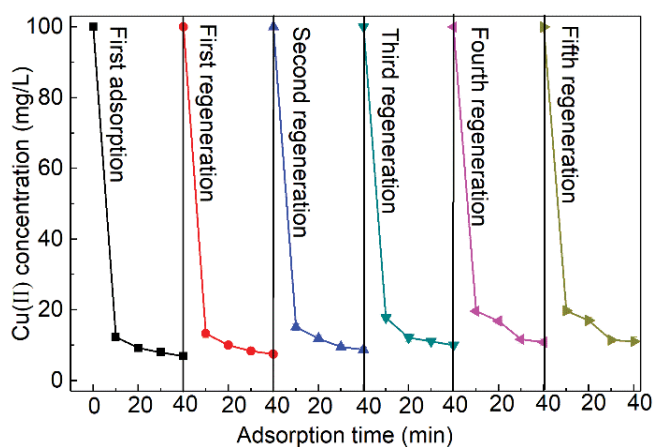


Fig. 10. Multiple adsorption curves of geopolymers.

investigated. Fig. 11a shows that the geopolymer maintained high adsorption performance after five regeneration cycles, achieving a removal efficiency of 95%. The corresponding immobilization efficiency was 99% (Fig. 11b). However, the weight of the geopolymer composite increased, resulting in a gradual decrease of immobilization efficiency.

3.8.2. Structure of the regenerated geopolymer

After five regeneration cycles, the crystalline state of the geopolymer did not strongly change, and the Na-PS crystal was the main type (Fig. 12). However, during the

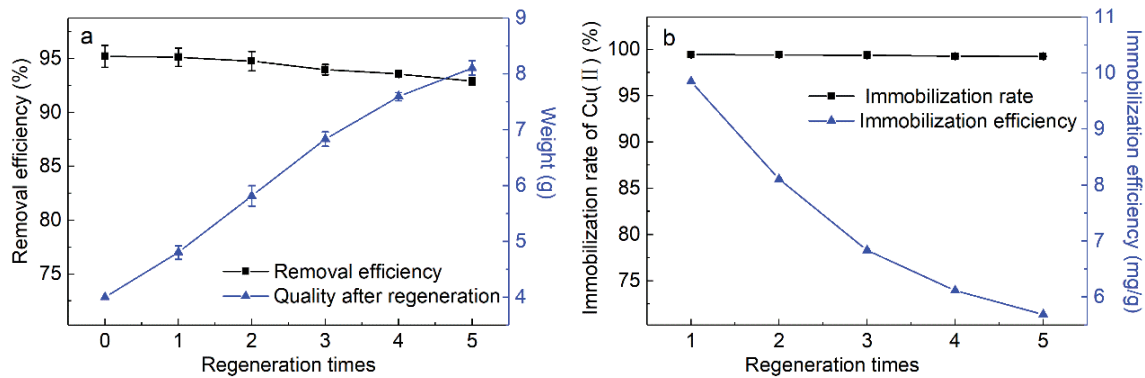


Fig. 11. Immobilization and regeneration of polymers.

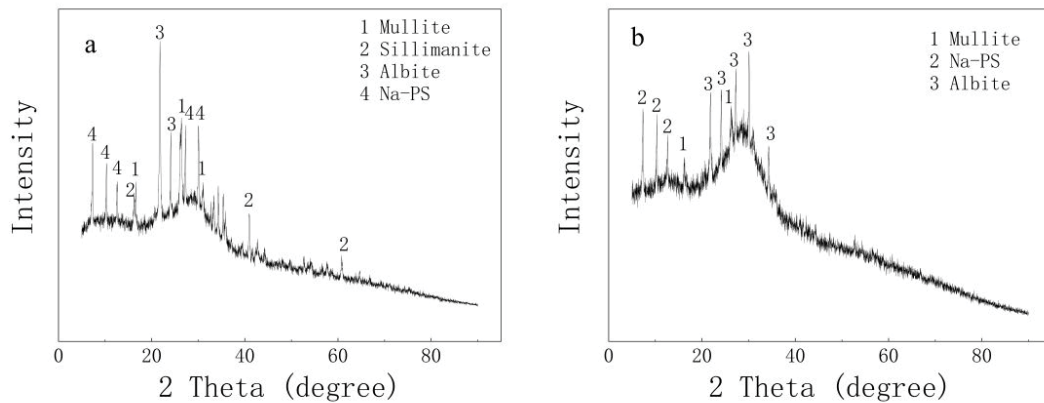


Fig. 12. XRD of regenerated polymer (a) first regeneration and (b) fifth regeneration.

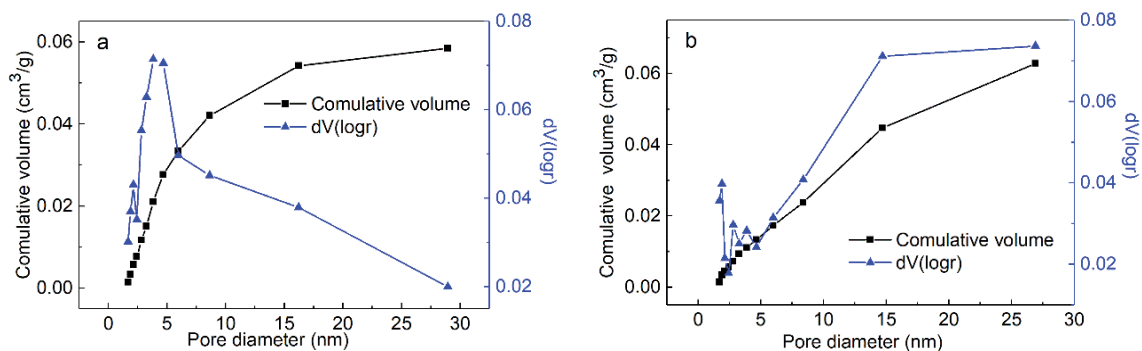


Fig. 13. Pore size distribution of geopolymer (a) first regeneration and (b) fifth regeneration.

regeneration process, the amount of silicon and aluminum gradually reduced, and albite was found in the samples. Moreover, the unreacted aluminosilicate components gradually transformed into geopolymers due to the activating agent. Albite formed due to the existence of sodium-containing activating agents (Na_2SiO_3 and NaOH).

The pore size distribution is presented in Fig. 13. In contrast to the geopolymer, recycled geopolymer was mainly mesoporous after the first regeneration, and the maximum and minimum pore sizes were 3.82 and 2.13 nm, respectively. Thus, the pore size of the recycled geopolymer was

significantly smaller. After the fifth regeneration, the pore size of the geopolymer further decreased. Moreover, Table 8 shows that after the first regeneration, the specific surface area of the geopolymer was reduced by half. However, there was no further change in the specific surface area of the geopolymer after repeated regenerations.

4. Conclusion

This study investigated the adsorption capacity of a metakaolin-derived geopolymer. The geopolymer was

Table 8
Pore size and specific surface area

Sample	Pore diameter range (nm)	Pore volume (cm ³ /g)	S _{BET} (m ² /g) (BET – Brunauer–Emmett–Teller)
Metakaolin	1.69–4.85	0.016	10.07
Geopolymer	2.47–15.98	0.078	32.16
First regeneration	2.13–3.82	0.058	16.28
Fifth regeneration	1.89–3.87	0.063	16.87

synthesized at an intermediate Al/Si ratio, and it exhibited high adsorption capacity under high alkalinity. The pore size distribution increased compared to those of raw materials. Batch tests indicated that the obtained geopolymer exhibited better Cu(II) removal efficiency compared to other geopolymer adsorbents. The adsorption process fitted well both the second-order model and Freundlich adsorption isotherm model. Furthermore, after five regenerations cycles, pore size decreased, but a high removal efficiency was maintained.

Acknowledgment

This work was supported by the Guangdong Science and Technology Department (2014A020209077).

References

- [1] S.F. Alshahateh, A.G. Jiries, S.A. Al-Trawneh, A.S. Eldouhaibi, M.M. Al-Mahadeen, Kinetic, equilibrium and selectivity studies of heavy metal ions (Pb(II), Co(II), Cu(II), Mn(II), and Zn(II)) removal from water using synthesized C-4-methoxyphenylcalix[4]resorcinarene adsorbent, *Desal. Water Treat.*, 57 (2016) 4512–4522.
- [2] L. Monser, N. Adhoum, Modified activated carbon for the removal of copper, zinc, chromium and cyanide from wastewater, *Sep. Purif. Technol.*, 26 (2002) 137–146.
- [3] A. Djukić, U. Jovanović, T. Tuvic, V. Andrić, J.G. Novaković, N. Ivanović, L. Matović, The potential of ball-milled Serbian natural clay for removal of heavy metal contaminants from wastewaters: simultaneous sorption of Ni, Cr, Cd and Pb ions, *Ceram. Int.*, 39 (2013) 7173–7178.
- [4] P. Duan, C.J. Yan, W. Zhou, D.M. Ren, Development of fly ash and iron ore tailing based porous geopolymer for removal of Cu(II) from wastewater, *Ceram. Int.*, 42 (2016) 13507–13518.
- [5] V.K. Gupta, M. Gupta, S. Sharma, Process development for the removal of lead and chromium from aqueous solutions using red mud—an aluminium industry waste, *Water Res.*, 35 (2001) 1125–1134.
- [6] A.B. Đukić, K.R. Kumrić, N.S. Vukelić, Z.S. Stojanović, M.D. Stojmenović, S.S. Milošević, L.L. Matović, Influence of ageing of milled clay and its composite with TiO₂ on the heavy metal adsorption characteristics, *Ceram. Int.*, 41 (2015) 5129–5137.
- [7] J. Davidovits, M. Davidovits, N. Davidovits, Process for Obtaining a Geopolymeric Aluminosilicate and Products Thus Obtained, US Patents, 1994.
- [8] Z.H. Zhang, H.J. Zhu, C.H. Zhou, H. Wang, Geopolymer from kaolin in China: an overview, *Appl. Clay Sci.*, 119 (2016) 31–41.
- [9] A. Singhal, B.P. Gangwar, J.M. Gayathry, CTAB modified large surface area nanoporous geopolymer with high adsorption capacity for copper ion removal, *Appl. Clay Sci.*, 150 (2017) 106–114.
- [10] J. Li, G.W. Yu, S.Y. Xie, L.J. Pan, C.X. Li, F.T. You, Y. Wang, Immobilization of heavy metals in ceramsite produced from sewage sludge biochar, *Sci. Total Environ.*, 628–629 (2018) 131–140.
- [11] Y.S. Zhang, W. Sun, Q.L. Chen, C. Lin, Synthesis and heavy metal immobilization behaviors of slag based geopolymer, *J. Hazard. Mater.*, 143 (2007) 206–213.
- [12] T. Bakharev, Geopolymeric materials prepared using Class F fly ash and elevated temperature curing, *Cem. Concr. Res.*, 35 (2005) 1224–1232.
- [13] M. Sarkar, K. Dana, S. Das, Microstructural and phase evolution in metakaolin geopolymers with different activators and added aluminosilicate fillers, *J. Mol. Struct.*, 1098 (2015) 110–118.
- [14] C.K. Yip, G.C. Lukey, J.L. Provis, J.S.J. van Deventer, Effect of calcium silicate sources on geopolymerisation, *Cem. Concr. Res.*, 38 (2008) 554–564.
- [15] J. Davidovits, Geopolymers: inorganic polymeric new materials, *J. Therm. Anal. Calorim.*, 37 (1991) 1633–1656.
- [16] Md. R. Awual, Md. M. Hasan, A novel fine-tuning mesoporous adsorbent for simultaneous lead(II) detection and removal from wastewater, *Sens. Actuators, B*, 202 (2014) 395–403.
- [17] Md. R. Awual, Md. M. Hasan, Fine-tuning mesoporous adsorbent for simultaneous ultra-trace palladium(II) detection, separation and recovery, *J. Ind. Eng. Chem.*, 21 (2015) 507–515.
- [18] Y.S. Ho, G. McKay, Pseudo-second order model for sorption processes, *Process Biochem.*, 34 (1999) 451–465.
- [19] S. Onutai, T. Kobayashi, P. Thavorniti, S. Jiemsirilers, Porous fly ash-based geopolymer composite fiber as an adsorbent for removal of heavy metal ions from wastewater, *Mater. Lett.*, 236 (2019) 30–33.
- [20] S. Andrejkovičová, A. Sudagar, J. Rocha, C. Patinha, W. Hajjaji, E.F. da Silva, A. Velosa, F. Rocha, The effect of natural zeolite on microstructure, mechanical and heavy metals adsorption properties of metakaolin based geopolymers, *Appl. Clay Sci.*, 126 (2016) 141–152.
- [21] M.S. Al-Harashsheh, K. Al Zboon, L. Al-Makhadmeh, M. Hararah, M. Mahasneh, Fly ash based geopolymer for heavy metal removal: a case study on copper removal, *J. Environ. Chem. Eng.*, 3 (2015) 1669–1677.
- [22] Z.X. Xiao, L.J. Zhang, L. Wu, D. Chen, Adsorptive removal of Cu(II) from aqueous solutions using a novel macroporous bead adsorbent based on poly(vinyl alcohol)/sodium alginate/KMnO₄ modified biochar, *J. Taiwan Inst. Chem. Eng.*, 102 (2019) 110–117.
- [23] S.Q. Tang, N.N. Shao, C.M. Zheng, F. Yan, Z.T. Zhang, Amino-functionalized sewage sludge-derived biochar as sustainable efficient adsorbent for Cu(II) removal, *Waste Manage.*, 90 (2019) 17–28.
- [24] S.M. Anush, B. Vishalakshi, Modified chitosan gel incorporated with magnetic nanoparticle for removal of Cu(II) and Cr(VI) from aqueous solution, *Int. J. Biol. Macromol.*, 133 (2019) 1051–1062.
- [25] X.-F. Sun, Y.W. Hao, Y.Y. Cao, Q.H. Zeng, Superadsorbent hydrogel based on lignin and montmorillonite for Cu(II) ions removal from aqueous solution, *Int. J. Biol. Macromol.*, 127 (2019) 511–519.
- [26] Md. R. Awual, Md. M. Hasan, Md. A. Khaleque, Md. C. Sheikh, Treatment of copper(II) containing wastewater by a newly developed ligand based facial conjugate materials, *Chem. Eng. J.*, 288 (2017) 368–376.

- [27] N.Y. Mezenner, A. Bensmaili, Kinetics and thermodynamic study of phosphate adsorption on iron hydroxide-eggshell waste, *Chem. Eng. J.*, 147 (2009) 87–96.
- [28] Y.S. Ho, G. McKay, Sorption of dye from aqueous solution by peat, *Chem. Eng. J.*, 70 (1998) 115–124.
- [29] O. Gulnaz, A. Kaya, F. Matyar, B. Arıkan, Sorption of basic dyes from aqueous solution by activated sludge, *J. Hazard. Mater.*, 108 (2004) 183–188.
- [30] Y. Yang, W.-q. Wu, H.-h. Zhou, Z.-y. Huang, T.-t. Ye, R. Liu, Y.-f. Kuang, Adsorption behavior of cross-linked chitosan modified by graphene oxide for Cu(II) removal, *J. Cent. South Univ.*, 21 (2014) 2826–2831.
- [31] S.J. Wu, F.L. Fu, Z.H. Cheng, B. Tang, Removal of Cr(VI) from wastewater by FeOOH supported on Amberlite IR120 resin, *Desal. Water Treat.*, 57 (2016) 17767–17773.